MAGNETIC RESONANCE IN MEDICINE

Theory of Heterogeneous Relaxation in Compartmentalized Tissues

Daniel Barsky, Benno Pütz, Klaus Schulten

A new model of compartmentalized relaxation—that which occurs for spins (protons) exchanging between compartments of different relaxation rates—is presented. This model generalizes previous ones by allowing spatially dependent relaxation within compartments. Solutions for the diffusion-Bloch equations are found via an efficient numerical technique known as the generalized moment expansion, and they agree well with the solutions to the standard two-site exchange equations (TSEE) for many typical situations. Specific models are developed for liposomes, red blood cells, capillaries, and arteries with respect to applied contrast agents. A parameter derived from tissue characteristics is introduced to predict the nature of the solutions. A new method is proposed for using contrast agents to detect capillaries, which exploits their high surface-to-volume ratio relative to the other elements of the vasculature.

Key words: capillary deletion; two-site exchange; contrast agents; generalized moment expansion.

INTRODUCTION

This paper provides a new model and mathematical techniques to describe the NMR signal under diffusional exchange between two or more compartments that differ in their relaxation rates and to delineate the implications of this model in terms of the discernible signal obtainable from tissue compartments such as capillaries.

Compartmentalized contrast agents act outside their compartments by the diffusion of water into or near the compartments. Indeed, we and others have shown that longitudinal relaxation rates T_1^{-1} measured for Gd-DTPA-filled liposomes and biological cells can be explained by water proton transport (exchange) across the cell membrane, and a quantitative description of this exchange mechanism has been worked out elsewhere (1–5). We and others have additionally addressed the enhancement of transverse relaxation rates T_2^{-1} by diffusion around cells or liposomes, which takes place in the presence of local field inhomogeneities due to susceptibility differences between cells or liposomes and the surrounding water (5–9). We consider here, however, only longitudinal relaxation, and at MRI field strengths (>1 T), there is no measurable analogue for enhanced longitudinal relaxation outside of large particles such as liposomes (7); thus it is the *exchange* mechanism of relaxation that we investigate here. The exchange mechanism has been exploited to measure diffusion across membranes according to various models (1–5, 10–17).

We have earlier developed a mathematical description for liposomes distributed in serum or tissue, based on the diffusion-Bloch (or Bloch-Torrey) equations and derived simple expressions, as well as spatially dependent expressions, that relate relaxation rates to liposome size and abundance as well as to a diffusion coefficient for water and liposomal membrane permeability (4). Other descriptions have included the strength (concentration) of the entrapped contrast agent by ignoring the spatial dependence of the relaxation—spins are regarded as either "in" or "out." This approach yields two coupled rate equations, often called the two-site exchange equations (TSEE, Eq. [6]). Such descriptions have been developed along various lines in (3, 5, 12) and applied toward permeability measurements of red blood cells in (13–17). More recently Herbst and Goldstein have reviewed the application of the TSEE in inferring the permeability of red blood cells in experiments where contrast agents are employed (18).

Here we investigate the limits of the TSEE model by developing a more general description that includes the spatial (radial) dependence of exchange, and we make comparisons for models of liposomes, red blood cells, and capillaries. We show how to predict the nature of the relaxation and when biexponential solutions can be simply related to exchange rates and to the physical volume fractions of the compartments. Finally, we show how a contrast agent could be used to detect viable capillary beds against the background of the rest of the vasculature.

METHODS

We employ a simple geometrical representation of cells, capillaries, and other tissue "vesicles" that have been presented with a contrast agent. We regard a tissue as a collection of biological vesicles embedded in a surrounding medium. Assuming a homogeneous distribution of cells or liposomes in tissue or serum, we model the entire tissue region by a single sphere of volume V which is divided into three concentric regions: a spherical interior radius r_1 that represents a cell or liposome, a surrounding shell of outer radius r_2 representing a membrane, and an outer region of radius r_3 representing the surrounding medium. In this model we make the assumption, as elsewhere (4, 19), that the spins diffusing through the outer region are reflected at half the average distance between vesicles r_3, which is given by

$$V = \frac{\text{total volume}}{\text{number of vesicles}} = \frac{4\pi}{3} r_3^3 \qquad [1]$$

MRM 37:666–675 (1997)

From the Department of Biophysics (D.B., K.S.), Physics (B.P., K.S.), and Beckman Institute (D.B., B.P., K.S.), University of Illinois at Urbana/Champaign, Urbana, Illinois.

Address correspondence to: Daniel Barsky, Ph.D., Sandia National Laboratory, P.O. Box, 969, M.S. 9214, Livermore, CA 94551.

Received July 12, 1996; revised September 16, 1996; October 17, 1996.

This work was completed at the National Institutes of Health's Resource for Concurrent Biological Computing (grant 1 P41 RR05969*01). One author (D.B.) was supported by an NIH training grant.

0740-3194/97 $3.00

Tubular vesicles such as arteries or capillaries will be regarded as locally parallel cylinders and thus treated as two-dimensional analogues of the cell model where "sphere" becomes "circle," and the volume V becomes area A. For simplicity of presentation we will develop the mathematics for the spherical geometry and explicitly mention cylindrical geometry only when the analogy might be lost.

Diffusion-Bloch Equations

We connect this geometrical model with the mathematical model developed by Bloch, and later modified by Torrey to describe the magnetization. Torrey suggested that when NMR is selective to water protons, the local magnetization is subject to the same diffusion law as the water molecules (20). Hence, he described each component of the local nuclear magnetization $\vec{m}(r, t)$ by the Bloch equations to which he added a diffusion term $\nabla \cdot D(r)\nabla$,

$$\partial_t \begin{pmatrix} m_{\text{trans}}(r,t) \\ m_{\text{long}}(r,t) \end{pmatrix} = \left[\nabla \cdot D(r)\nabla - \begin{pmatrix} i\omega_0 + T_2^{-1}(r) \\ T_1^{-1}(r) \end{pmatrix} \right] \cdot \begin{pmatrix} m_{\text{trans}}(r,t) \\ m_{\text{long}}(r,t) \end{pmatrix} \quad [2]$$

where $D(r)$ is the local diffusion coefficient of water, ω_0 is the Larmor frequency, and $T_2^{-1}(r)$, $T_1^{-1}(r)$ are the transverse and longitudinal uncompartmentalized relaxation rates, i.e., for a solution of contrast agent or in plain water in the absence of proton exchange between environments. The spatial dependence of these rates will be simple radial step functions of the short and long relaxation times in the presence and absence of a contrast agent, respectively.

For concreteness we consider mainly a T_1-weighted, inversion-recovery scheme. For this case we solve the equation which describes the longitudinal magnetization, although the transverse magnetization follows a similar description.[1] In an alternative notation, where $\mathcal{D}(r)=\nabla \cdot D(r)\nabla$, $k(r)=T_1^{-1}(r)$ and $m(r, t) = m_{\text{long}}(r, t)$, the longitudinal magnetization from Eq. [2] is written

$$\partial_t m(r,t) = [\mathcal{D}(r) - k(r)]m(r,t) \quad [3]$$

The physical observable is the overall magnetization, obtained by integrating over all space $M(t) = \int_0^{\infty} d\Omega\, m(r,t)$ where $d\Omega$ is a differential surface or volume element for two- or three-dimensional geometries, respectively.

In an inversion-recovery sequence, the initial conditions are of a uniform magnetization, inverted relative to the equilibrium magnetization; i.e., at time $t = 0$ an instantaneous, nonselective 180°-pulse is applied. For convenience we use a transformed, normalized local magnetization $m(r, t)$ which relaxes from unity to zero, so that if m' denotes the actual local magnetization and m'_{eq} denotes the actual (uniform) equilibrium magnetization, then

$$m(r,t) \equiv \frac{1}{2}\left[1 - \frac{m'(r,t)}{m'_{\text{eq}}}\right] \quad [4]$$

The initial conditions are then

$$m'(r,t=0) = -m'_{\text{eq}} \quad \text{and} \quad m(r,t=0) = 1 \quad [5]$$

Two-Site Exchange Equations

Rather than solving Eq. [3] directly, one can describe the magnetization of a two compartment system by two components, m_i and m_o, corresponding, for example, to the magnetization of spins inside and outside the liposome, respectively. If τ_{io} and τ_{oi} represent the average time for water molecules to cross the membrane from the inside and the outside, respectively, and the local relaxation times inside and outside are denoted by T_i and T_o, then this two site description can be formulated in a system of coupled differential equations, the two site exchange equations (TSEE, cf. (17, 18))

$$\frac{d}{dt}\begin{pmatrix} m_i(t) \\ m_o(t) \end{pmatrix} = \underbrace{\begin{pmatrix} -(R_i + \tau_{io}^{-1}) & \tau_{io}^{-1} \\ \tau_{oi}^{-1} & -(R_o + \tau_{oi}^{-1}) \end{pmatrix}}_{\mathcal{R}} \begin{pmatrix} m_i(t) \\ m_o(t) \end{pmatrix} \quad [6]$$

where R_i and R_o are the "inside" and "outside" relaxation rates, respectively. If, for example, the contrast agent is present only in the inside compartment, then $R_i = T_{\text{agent}}^{-1} + T_1^{-1}$ and $R_o = T_1^{-1}$ where T_{agent}^{-1} is the relaxation rate enhancement due to the same concentration of contrast agent in an uncompartmentalized system. As an initial condition we choose, without loss of generality, the total magnetization $m_i(0) + m_o(0)$ normalized to unity. It is useful to define a volume fraction V_f as the ratio of the inside compartment volume V_i to the total volume V,

$$V_f = \frac{V_i}{V} = \frac{m_i(0)}{m_o(0) + m_i(0)} = \left(\frac{r_1}{r_3}\right)^3 \quad [7]$$

Using a modern mathematics software package, is easy to obtain the solution to Eq. [6]. We have included a short *Mathematica* script in Appendix A. The solutions to Eq. [6] have been published in (17), as well as the less accessible algebraic inverse thereof. In principle, the inverse solutions transform the measured biexponential rates and components into physical volume fractions and membrane transit rates, i.e., membrane permeabilities.

A well-known formula relates the exchange rate τ_{io}^{-1} to the permeability P_d of the barrier,

$$\tau_{io}^{-1} = P_d \frac{V_j}{S_j} \quad [8]$$

where S_j is the surface area of compartment j. Equation [8] has been derived in ref. 4, and it is valid as long as the diffusion constant of water through the barrier membrane D_m is much smaller than the diffusion constant of water D_w. For a membrane of thickness d, $D_m = P_d d$. Detailed

[1] The transverse magnetization can be described in exactly the same way if one applies a transformation $m_{\text{trans}}(r, t) = e^{-i\omega_0 t}m(r, t)$, which is valid in the absence of non-discountable (via spin-echo, etc.) field inhomogeneities. Such non-discountable inhomogeneities will occur in the case of superparamagnetic contrast agents and may appear due to susceptibility effects outside of Gd-filled vesicles, although such effects are normally negligible (5).

balance demands that a particle exit for every one that enters, so that $\tau_{oi}^{-1} = V_f \tau_{io}^{-1}$.

Finite Difference Approximation

It is also desirable to solve Eq. [3] directly. To this end we make a finite difference approximation to Eq. [3], whereby the diffusion space of radius R is discretized and, by the spherical symmetry, mapped onto an N-dimensional vector $\mathbf{r}$ with components $\{r_n = nR/N$ for $n = 1, \ldots, N\}$ that correspond to discrete shells of the spherical diffusion space. (To avoid confusion R is used here in place of r_3 of the last section.) The choice of N determines the smoothness of the approximation; all calculations presented here have employed $N = 1000$. The local magnetization $m(r, t)$ is approximated by an N-dimensional vector $\mathbf{m}(t)$ where the nth component is defined by

$$m_n(t) \equiv m(r = r_n, t)v_n \qquad [9]$$

where

$$v_n \equiv \left(\frac{4\pi}{3}\right) \frac{r_n^3 - r_{n-1}^3}{V} \qquad [10]$$

For each $n \in [1, N]$, v_n is proportional to the volume of the shell between radii r_{n-1} and r_n, and we called the vector $\mathbf{v}$, of which the v_n are components, a volume distribution vector.

According to Eq. [9], the initial condition for the local magnetization (Eq. [5], right) is $\mathbf{m}(t = 0) = \mathbf{v}$. Thus, the nth component of $\mathbf{m}(t = 0)$ is determined by the equilibrium distribution of particles

$$m_n(t = 0) = v_n = \frac{n^3 - (n-1)^3}{N^3} \qquad [11]$$

The Brownian motion of the water protons is represented by "jumps" between adjacent shells, e.g., from r_n to $r_{n\pm1}$. The rapidity of these jumps is determined by an $N \times N$, tridiagonal transition matrix $\mathbf{D}$ (defined below) which replaces the differential diffusion operator $\mathcal{D}(r)$ (21, 22). Similarly, the scalar reaction operator $k(r)$, defined by Eq. [3], is mapped onto a diagonal matrix $\mathbf{K}$ with nonvanishing elements $K_{nn} = k(r = r_n)$. If $k(r)$ is not constant within a particular shell, the volume-averaged value in that shell is taken. With this notation the master equation corresponding to Eq. [3], i.e., the finite difference approximation to Eq. [3], can be written

$$\partial_t \mathbf{m}(t) = [\mathbf{D} - \mathbf{K}]\mathbf{m}(t) \qquad [12]$$

The overall magnetization $M(t)$ is the sum over the components of $\mathbf{m}(t)$,

$$M(t) = \sum_{n=1}^{N} m_n(t) \qquad [13]$$

and the actual magnetization $M'(t)$ can be determined by analogy to Eq. 4, $M'(t) = m'_{eq}(1 - 2M(t))$.

Transition Matrix

For the discretization scheme described above the transition matrix $\mathbf{D}$ is tridiagonal and is defined by (21–23)

$$D_{jk} = \begin{cases} -(D_{k-1,k} + D_{k+1,k}) & j = k \\ \tau^{-1}\sqrt{v_j/v_k} & j = k \pm 1 \\ 0 & \text{otherwise} \end{cases} \qquad [14]$$

where the indices $j, k \in [1, N]$, and elements with an index of zero or $N + 1$ are taken to be zero. The latter assumptions are in accordance with the conservation of particles at the origin and with the reflection of particles at the outer boundary R (22). For each j, k pair, $\tau^{-1}\sqrt{v_j/v_k}$ denotes the jump rate from site r_k to r_j. This rate is related to the diffusion coefficient $D(r)$ by $\tau^{-1}(r) = D(r)/(R/N)^2$, which describes the finite difference analogue to Einstein's diffusion equation (24). In this representation the off-diagonal elements D_{jk} control the diffusion from site r_k to r_j, and the diagonal elements L_{jj} account for the flow from site r_j to sites r_{j-1} and r_{j+1}. At the membrane interfaces the diffusion coefficient abruptly changes. We take the volume-weighted average of the two rates for those lattice sites which contain both membrane and surrounding medium.

The existence of an equilibrium distribution, namely $m_j(t) = v_j$, requires that the condition of detailed balance be satisfied

$$D_{jk}v_k = D_{kj}v_j \qquad [15]$$

It can easily be verified that the transition matrix (14) satisfies condition (15).

Solution by Newton's Method

By an approximation known as Newton's method, a time-iterative solution of Eq. [12] can be obtained according to the scheme

$$\mathbf{m}(t + \Delta t) \simeq \mathbf{m}(t) + \Delta t(\mathbf{D} - \mathbf{K})\mathbf{m}(t) \qquad [16]$$

where Δt denotes a short time interval. Starting with $\mathbf{m}(t = 0)$ as given by Eq. [11] and taking Δt sufficiently small, one can iteratively evaluate $\mathbf{m}(t)$ for arbitrarily long times. To this solution we can fit a mono-, bi-, or multi-exponential curve and, thereby, find the corresponding rate(s). For example, one can measure the very early and very late slopes of a semi-log plot to obtain the rates of a biexponential fit.

Generalized Moment Expansion

When it is known that the solution is a sum of exponentials, then the generalized moment expansion (GME) is much more efficient than Newton's method. The GME has been thoroughly described elsewhere where it has been applied to Brownian relaxation processes (21), dynamic correlation functions (25), and used to develop the method of continuous microphotolysis (FRAP) (26, 27).

The method is related to the Mori-Zwanzig formalism (refs. given in (26)). It involves projection of m(t) onto the subspace of selected low and high frequency modes. In an appendix we provide the detailed mathematical for-

mulation of the method, and give explicit expressions for amplitudes and relaxation times corresponding to mono- and biexponential descriptions. The method requires a calculation of the short and long time moments μ_i which, respectively, characterize the fast and slow responses of $M(t)$. The derived moments are used to construct a Padé approximant which yields a multiexponential (here biexponential) solution. A monoexponential solution requires two moments, e.g., μ_0, μ_{-1} which reproduce $M(0)$ and $\int_0^\infty dt\, M(t)$ exactly. A biexponential solution requires four moments, e.g., μ_1, μ_0, μ_{-1}, μ_{-2} which reproduce $M'(0)$, $M(0)$, $\int_0^\infty dt\, M(t)$, and $\int_0^\infty dtt\, M(t)$ exactly. If, however, the moments are proportional to one another, the solution will be mono-exponential, and the biexponential solution will encounter a singularity. The choice of moments depends on what one intends to describe best: positive moments provide a description which is more accurate for short times $t \simeq 0$, while negative moments provide a description more accurate for long times, $t \gg 0$. The GME is several orders of magnitude faster than Newton's method where Δt must be chosen much smaller than any of the relevant time constants, r_3^2/D_w, τ_{io}, τ_{oi}, and T_{agent}.

Model Applications

We employ the TSEE and the GME algorithms described above to obtain the longitudinal magnetization as a function of time for model systems. The monoexponential descriptions are obtained via Eqs. [B12] and [B14], using the moments μ_0 and μ_{-1}. For the GME biexponential solutions, the μ_{-3}, μ_{-2}, μ_{-1}, μ_0 moments of the GME are inserted into Eqs. [B15–B19].

Liposomes and Cells

We consider two experimentally relevant liposomal systems whose characteristics are listed in Table 1: a paramagnetic contrast agent (e.g., Gd-DTPA) entrapped in liposomes that are suspended in water or serum which is free of contrast agent (row 1, "ensomes"); and water-filled, contrast agent-free liposomes suspended in a solution of contrast agent (row 2, "exsomes").

We employ the same (0.3%) concentration of liposomes as used experimentally in refs. 28 and 29. The liposomes are assumed to have a uniform radius of r_2 = 50 nm, including the membrane, and a membrane thickness of d = 5 nm. The contrast agent is assumed to provide an enhanced relaxation rate four orders of magnitude larger than the native relaxation rate T_1^{-1} which was taken to be 0.3 s^{-1}. In particular, in 670 mM Gd-DTPA the relaxation rate has been measured at 1869 s^{-1} (28).

For the ensomes we used the experimental parameters published in ref. 28 and reproduce the experimental value of the measured (slow) relaxation rate, 2.5 s^{-1} (28), after additionally assuming a value $D_m = 8 \times 10^{-14}$ m^2/s, which is reasonable for the egg-PC liposomes at room temperature (30). For considerably more impermeable DPPC/DPPG exsomes, we assumed $D_m = 9 \times 10^{-17}$ m^2/s to reproduce the experimentally observed slow relaxation component of 1.5 s^{-1} (30). Although the other parameters were not published for this experiment, this D_m value is entirely consistent with published values for DPPC/DPPG liposomes (30).

The red blood cells are modelled as spheres for the purpose of employing the finite difference approximation, but this should have little effect on the solution results as long as the cells are randomly oriented. In the TSEE description shape is not a factor at all. Many investigators have reported using a contrast agent (usually Mn^{2+}) to measure red blood cell permeability (13–17), using TSEE and various approximations thereof. An excellent review is available (18). In Table 1, rows 3a and 3b, we have selected parameters to demonstrate the effects of high and low levels of contrast agent and to compare the TSEE and GME solutions.

Capillaries and arterioles

The capillary model we present here is a two-dimensional model which describes tissue in terms of capillaries, lumen, and a homogeneous intercapillary medium. For the moment we ignore the presence of other, differently-sized blood vessels such as arterioles. The methods are the same as in the Methods section, except that the volume V (Eq. [1]) is replaced by an area $A = \pi R^2$ and Eqs. [10] and [11] are modified accordingly.

Capillaries come in highly varying types and characteristics, liver capillaries being the most permeable, brain capillaries the least, and muscle capillaries in between (31). The permeability P_d of a membrane to a substance is related to an effective diffusion coefficient D_m of that substance in the membrane by

$$P_d = \frac{D_m}{d} \qquad [17]$$

Table 1
The Physical Parameters Used in Table 2

	System	V_f	r_1[m]	d[nm]	R_i [s^{-1}]	R_o [s^{-1}]	D_m [10^{-14} m^2/s]	D_w [10^{-14} m^2/s]
1	Ensomes	0.003	45 10^{-9}	5	1869	0.3	8	2.3
2	Exsomes	0.01	45 10^{-9}	5	0.3	100	0.009	2.3
3a	Blood cells	0.1	5 10^{-6}	10	2	20	20	2.3
3b	Blood cells	0.1	5 10^{-6}	10	2	1000	20	2.3
4	Imperm. capil.	0.04	2.5 10^{-6}	10	100	1	1	1
5	Semi. capil.	0.04	2.5 10^{-6}	10	100	1	20	1
6	Perm. capil.	0.04	2.5 10^{-6}	10	100	1	100	1
7	Arteriols	0.1	25 10^{-6}	20	100	1	20	1
8	Arteries	0.1	250 10^{-6}	100	100	1	20	1

where d denotes the thickness of the membrane. The capillary wall can be modeled in two different ways: as two lipid bilayers each about 5-nm thick, separated by a 1 μm thick layer of cytoplasm or as a single, homogeneous layer of low diffusivity. The diffusivity values D_m are determined by the published values of P_d, using Eq. [17]. For brain capillaries a water-through-membrane permeability in the range 6×10^{-3} to 2×10^{-4} cm/s (D_m = 60 to 2 [$\times 10^{-14}$ m^2/s]) probably exists as long as the blood-brain barrier (BBB) remains intact (32–34). A breakdown of the BBB could either increase permeability to water or Gd-DTPA or both. If the Gd-DTPA leaks out of the capillary space, then the decay is expected to become everywhere enhanced and lose its biexponentiality. This by itself appears to have diagnostic value, e.g., in the assessment of insults to the brain, but it makes it impossible to distinguish the intra-capillary signal from the inter-capillary signal.

Values for average capillary volume are in the range of 4% to 7% of the total brain volume (35, p. 311). The employed parameters for capillaries and larger blood vessels are listed in rows 4–8 of Table 1. We employ a range of experimental possibilities for purposes of comparison.

RESULTS AND DISCUSSION

We have solved Eq. [3] (GME) and Eq. [6] (TSEE) for the previously described models of liposomal systems, red blood cells, capillaries, arterioles, and arteries under the initial conditions of an inversion-recovery experiment (Eq. [5]). Using the parameters listed in Table 1, we present the solutions in Table 2.

TSEE versus Finite Difference Methods

Inspection of Table 2 reveals that the TSEE and the biexponential GME agree well for all situations considered here. We conclude that a model with radial dependence is unnecessary for these applications because the relaxation depends only on exchange. Changing the membrane thickness, for example, from d = 10 nm to d = 1 μm—and rescaling D_m accordingly—produces the same results in our capillary model. Nevertheless, where compartmental division is weak or lacking (i.e., $D_m \simeq D_w$), Eq. [8] will not be valid (4), and an exchange model becomes inappropriate. For uniform initial conditions the relaxation will be monoexponential, but where the magnetization is not everywhere the same at time $t = 0$, the finite difference methods developed here can be used to describe the behavior of the magnetization.

The Characterization of Relaxation

Intercompartmental exchange can be characterized as slow, intermediate, and fast. Under fast exchange, the relaxation will be monoexponential, with the single rate being the weighted volume-average of the two rates. Under slow exchange the relaxation will be "simple biexponential," i.e., relative components of the signal will correspond closely to the volume fractions of the physical compartments. Under intermediate exchange the relaxation will be biexponential, but the relaxation components do not directly correspond to the physical volume fractions; they are related by complicated algebraic expressions (17).

Mathematically, Eq. [6] yields a biexponential solution for the magnetization decay

Table 2
Relaxation of Several Physical Systems Involving Compartmentalized Contrast Agents

	System	Q	TSEE	GME	
				bi	mono
1	Ensomes	0.57	0.1%:2940 99.9%:2.34	0.1%:2747 99.9%:2.47	2.47
2	Exsomes	0.01	99.0%:100.3 1.0%:1.50	98.7%:99.7 1.2%:1.50	54.5
3a	Blood cells	1.7	45.1%:12.2 54.9%:23.1	43.8%:12.1 56.2%:23.0	16.5
3b	Blood cells	0.01	89.8%:1001 10.2%:14.0	89.8%:1001 10.2%:13.8	121
4	Imperm. capil.	0.008	3.9%:101.8 96.1%:1.03	3.9%:100.8 96.1%:1.03	1.07
5	Semi. capil.	0.17	3.0%:117 97.0%:1.55	3.0%:114 97.0%:1.54	1.59
6	Perm. capil.	0.84	1.2%:182 98.8%:2.83	1.6%:145 98.4%:2.55	2.59
7	Arteriols	0.009	9.8%:101 90.2%:1.09	9.97%:84.4 90.0%:1.07	1.19
8	Arteries	0.0002	10.0%:100.0 90.0%:1.00	9.99%:97.5 90.0%:1.00	1.11

(1) Liposomes entrapping contrast agent, (2) liposomes excluding contrast agent, (3) blood cells in a bath of contrast agent (analogous to exsomes), and, all entrapping contrast agent, (4) impermeable, (5) semi-permeable, and (6) highly permeable capillaries, (7) arterioles, and (8) arteries. Biexponential descriptions are given in terms of two amplitudes each followed by a respective rate. Thus the expression 0.001 exp(−3060t) + 0.999 exp(−2.48t) is written 0.1%:3060; 99.9%:2.48. The monoexponential rates (last column) are calculated from μ_0/μ_{-1} (see Discussion). All rates are in s^{-1}. The physical parameters are listed in Table 1.

$$m(t) = m_1 \exp(-R_{slow}t) + m_2 \exp(-R_{fast}t) \quad [18]$$

and the eigenvalues of $\mathcal{R}$ constitute the two rates R_{slow} and R_{fast} while the magnitude of the eigenvectors of $\mathcal{R}$ describe the relative populations m_1 and m_2 relaxing at those rates. If τ_{io}^{-1} and τ_{oi}^{-1} were zero (i.e., no exchange) then the rates R_{slow} and R_{fast} would just be the two diagonal elements R_i and R_o, and the components m_1 and m_2 would exactly correspond to $m_i(0)$ and $m_o(0)$. We call such behavior simple biexponential. The greater the amount of exchange, the less these correspondences hold.

We have developed a simple diagnostic for determining the exchange condition. We first define the quantity Q, which relates to the diagonality of $\mathcal{R}$.

$$Q = \begin{cases} \dfrac{\tau_{io}^{-1}/(1-V_f)}{(R_o - R_i)}, & R_i < R_o \\ \dfrac{\tau_{oi}^{-1}/V_f}{(R_i - R_o)}, & R_i > R_o \end{cases} \quad [19]$$

If Q is much greater than unity ($Q > 10$), then the exchange is fast and the relaxation is monoexponential. If Q is much less than unity ($Q < 0.1$), then the exchange is slow and the relaxation is simple biexponential. Finally, if Q is within an order of magnitude or so of unity ($0.1 < Q < 10$) then there is intermediate exchange and the relaxation is biexponential with the relaxation components being related to the physical compartments in an algebraically complicated way.

Monoexponential Relaxation

An exception to this last rule occurs when the compartment with the fast relaxation is very small (<1%), in which case the slower component of the biexponential relaxation will dominate, and the relaxation is practically monoexponential; i.e., the slow rate is equal to the monoexponential rate as in row 1 in Table 2. In an experiment the measured data is usually fit to a monoexponential or biexponential decay curve by a least squares fit. Since all of the Q values in Table 2 are much less than 10, none of the decays are properly described by a monoexponential function. Nevertheless, the fast component is often not measured because the data are collected at times much later than the fast relaxation time; thus mostly the slow component of the relaxation is observed. In Table 2 the monoexponential rates demonstrate the inadequacy of a monoexponential description. The rates have been determined by the ratio μ_0/μ_{-1} which provides a compromise between the short-time and the long-time behavior. What would be observed experimentally depends on when during the relaxation the data are collected. A monoexponential fit to highly relaxed data would be better predicted by the long-time moments, e.g., the ratio μ_{-3}/μ_{-4}; such ratios converge to the slow rate with successively more negative moments.

Biexponential Relaxation

In the case of slow exchange ($Q < 0.1$), the relaxation is simple biexponential, which implies that not only are the physical volume fractions simply given by the relaxation components, but the measured relaxation rates are easily related to the membrane permeability and vesicle size (or surface-to-volume ratio). Under slow exchange, the slower of the measured decay rates closely corresponds to the membrane exchange rate from the slow to the fast compartment; i.e., it holds that

$$R_{slow} - T_1^{-1} \simeq \begin{cases} \tau_{io}^{-1}, & R_i < R_o \\ \tau_{oi}^{-1}, & R_i > R_o \end{cases} \quad [20]$$

Conlon and Outhred employed this approximation (together with Eq. [8]) in their original study of water diffusion permeability of erythrocytes using NMR (36). In their review Herbst and Goldstein (18) indicate that Eq. [20] is made less accurate by finite fast relaxation rates (i.e., finite Mn^{2+} concentrations) and point out the insufficiency of patching this approximation with a "backflux term," but stop short of presenting a diagnostic such as Q which determines the validity of Eq. [20]. The results for model red blood cells (rows 3a and 3b) illustrate the effect of finite Mn^{2+} concentrations: in row 3a the components m_1 and m_2 are very different from m_i and m_o. In this case, however, $R_{slow} - T_1^{-1}$ is only 13% less than τ_{io}, implying that the membrane permeability would be undervalued by only about 13%.

When the exchange is intermediate ($0.1 < Q < 10$), one may resort to solving Eq. [6] for $m_i(0)$ and $m_o(0)$ in terms of the the fast and slow rates and amplitudes (17), but the equations are complex, highly non-linear function of input parameters such as vesicle radius and membrane permeability. The uncertainties in the biexponential fit will further diminish the reliability of such an approach (37).

3.3 Observing Small Vessels

For many applications it is necessary to be able to distinguish the intra-capillary signal from extra-capillary signal. On the one hand, if resolution is great enough, such as the several micron resolution available in NMR microscopes (presently in vitro only), one can expect to visualize capillaries directly. On the other hand, at clinical resolution, which is on the order of millimeters, an indirect method for visualizing capillary beds can be employed as will be described.

Signal from Capillaries

When there is slow or intermediate exchange, a monoexponential description ignores the fast component of the relaxation. Our capillary model (rows 4–6) shows that the monoexponential rates are very close to the slow component rates of the biexponential solutions, which would seem to imply that the fast component can be ignored. By an appropriate experimental method, however, the fast component may be measurable, and this component is related to the intracapillary signal as described above. In Fig. 1 we present the magnetization recovery in time as a function of distance from the center of a model capillary, as would occur during an inversion-recovery experiment. One can observe that signal contrast between the signal from the capillaries and the

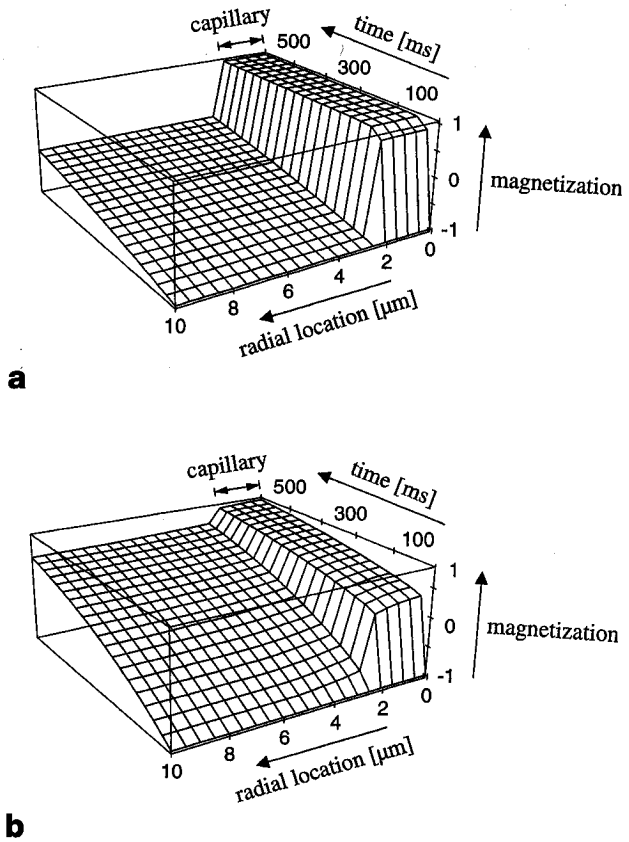

FIG. 1. Magnetization (normalized) as a function of time and distance from the center of a model capillary containing Gd-DTPA. The two figures differ only by the permeability of the capillary membrane: (a) row 4 and (b) row 6 in Table 1. Even for the highly permeable capillary (b), there is strong signal contrast between the intracapillary and the extracapillary signal for 10 to 100 ms.

surrounding tissue is maximal within tens of milliseconds after a 180°-preparation pulse. This assumes that transport through capillary walls is the dominant mechanism of spin-lattice (T_1) relaxation enhancement; and susceptibility effects can be minimized by keeping the acquisition time TI, during which spin-spin (T_2) relaxation occurs, quite short (to less than about 20 ms). In Fig. 1a the water permeability of the capillary wall is low ($P_d = 10^{-4}$ cm/s), and there is a sharp division between the magnetization inside and outside the capillary that persists for hundreds of milliseconds. Figure 1b demonstrates, however, that even for much more permeable capillaries ($P_d = 10^{-2}$ cm/s), strong signal contrast is available from an inversion-recovery imaging sequence if *TI* is in the range of 50 to 200 ms.

Inversion-recovery bears the disadvantage that one must wait for the extracapillary signal to go through a null before probing the intracapillary signal with a 90°-pulse. Another way is to apply a 90°-τ-180°-τ-90° pulse sequence such that τ is only a few milliseconds, on the order of the agent relaxation time T_{agent}. In this sequence, at time 2τ most of the spins in the intercapillary region would be refocused by the 180°-pulse, while most spins in the intracapillary region would be fully relaxed—realigned with the external magnetic field. Since the second 90°-pulse comes at the echo time of the mostly unrelaxed spins (intercapillary) spins, they are inverted at the same time that the intracapillary are excited by the second 90°-pulse.

Signal from Capillary Beds

Since the relaxation rates are primarily exchange controlled, the measured relaxation rates depend sensitively on the exchange rates for the spins between the intra- and inter-capillary spaces. Since the exchange rates depend linearly on the surface-to-volume ratio of the vesicles, the much wider (10×) arterioles and (100×) arteries give rise to a much less enhanced surrounding relaxation rate. In other words, $R^{slow}_{capillary} \gg R^{slow}_{arteriole}$. This is supported by the slow rates in rows 5 and 6 versus those in rows 7 and 8 of Table 2. The important implication is that by looking at the slow component of the relaxation, a region containing capillaries will show markedly faster relaxation than regions of only arterioles and arteries.

To exploit the difference in the two decay rates between regions containing viable capillaries and those that do not, we propose another WEFT-like inversion-recovery sequence whereby the signal of the more slowly decaying region is eliminated, revealing the capillary-bed signal. Where capillaries are present, the slow component will be dominated by the capillary-enhanced relaxation, and only regions where capillaries are not present (or are unable to pass contrast agent-containing lumen) should appear dark. The fraction of signal left I_{WEFT} in such an experiment is given by

$$I_{WEFT} = 1 - 2\exp\left[- ln(2)\frac{R^{capillary}_{slow}}{R^{arteriole}_{slow}}\right] \qquad [21]$$

For example, 25% of the signal from capillary beds such as in row 5 should be detectable at the moment the signal is null from regions of only arterioles such as in row 7. Where possible, it may also be advisable to examine images obtained with and without contrast agent.

CONCLUSION

We have presented a simple model of compartmentalized relaxation in a variety of biological contexts. We have shown that ordinarily, liposomes entrapping a contrast agent produce monoexponential relaxation, red blood cells in a medium doped with a contrast agent produce biexponential relaxation, and capillaries conducting a contrast agent produce biexponential relaxation.

For simple geometries and uniform initial conditions, we have found no advantage in employing a spatially dependent model; both the TSEE and the GME descriptions agree well for the cases examined. For highly convolved shapes and/or non-uniform initial conditions, one can proceed from Eq. [12] to solve $\mathbf{m}(t)$ on a lattice of two or more dimensions.

When very high resolution NMR is available, an inversion recovery sequence with a very short TI or a modified inversion-recovery scheme have been proposed here to capture the fast relaxing component of capillaries. The fast relaxing component, however, will be due to all

regions where the contrast agent is present, including the rest of the vasculature. Because the present model considers only movement perpendicular to each capillary axis (i.e., not flow), flow isolation techniques could be used to differentiate capillary and arterial blood in addition to the method of presented here of using contrast agents (or other relaxation differential) to distinguish the intra- and inter-capillary lumen.

Fortunately, although the small size of capillaries makes it infeasible to image them individually in a clinical setting, their high surface-to-volume ratio gives rise to alternate route to their detection: Capillaries conducting a contrast agent will more greatly enhance the relaxation of the surrounding tissue than the much larger parts of the vasculature. We suggest that by detecting the slowly relaxing component while suppressing the even more slowly relaxing signal from the surrounding tissue, regions of viable capillaries should become pronounced.

APPENDIX A: TSEE BY MATHEMATICA

The following *Mathematica* commands define a function TSEE to solve Eq. [6] for two spin populations which inter-exchange and relax at different rates.

```
TSEE[Vf_,r1_,d_,Ri_,Ro_,Rn_,Dm_]: =
Module [{Ci,Co,Rio,Roi},
Rio = (2 Dm)/(r1 d); (*2 for cylinders, 3 for spheres *)
Roi = Vf Rio;
fullsol = DSolve[{ - (Ri + Rio + Rn)*Ci[t] + Roi*Co[t] == Ci'[t],
        Rio*Ci[t] + - (Ro + Roi + Rn)*Co[t] == Co'[t],
        Ci[0] == Vf, Co[0] == (1 - Vf)}, {Ci[t],Co[t]},t];
        Return[Simplify[Evaluate[Ci[t] + Co[t]/.fullsol]]];]
```

The parameters used in TSEE are: Vf the volume fraction of the capillaries, r1 the radius of the capillaries, d the thickness of the capillary membrane, Ri the relaxation rate inside the capillary, Ro the relaxation rate outside the capillary, Rn the native relaxation rate, and Dm the diffusion constant in the capillary membrane. The internal variables Ci and Co denote the magnetization signal from inside and outside the capillary, respectively, and Rio and Roi are the exchange rates across the wall, from inside to outside and vice versa, respectively.

As an example, we apply the TSEE program to capillaries, by issuing the command "TSEE[0.04, 2.5 10^−6, 10 10^−9, 100, 0, 1, 20 10^−14]". This produces the output, "$\left\{\frac{0.0298492}{E^{117.089\,t}} + \frac{0.970151}{E^{1.5513\,t}}\right\}$."

APPENDIX B GENERALIZED MOMENT EXPANSION (GME)

This is a brief summary of the algorithm presented in refs. 21, 25, 26, applied here to the diffusion-Bloch Eq. [3] and to the observable $M(t)$ (Eq. [13]).

Determination of the Moments

A Laplace transform of Eq. [12] produces the following expression for the magnetization in frequency space

$$\hat{M}(\omega) = \int_0^\infty dt\, \exp(-\omega t)\, M(t) \qquad [B1]$$

$$= \eta[\omega \mathbf{1} - (\mathbf{D} - \mathbf{K})]^{-1}\, \mathbf{m}(0) \qquad [B2]$$

where we have introduced a row vector $\eta = (1, 1, 1, \ldots)$. We apply the GME to $\hat{M}(\omega)$, expanding it about $\omega = 0$ and $\omega = \infty$

$$\hat{M}(\omega) = \sum_{\nu=0}^{\infty} \mu_{-\nu-1}(-\omega)^\nu \quad \text{as} \quad \omega \to 0, \qquad [B3]$$

$$\hat{M}(\omega) = \frac{1}{\omega}\sum_{\nu=0}^{\infty} \mu_\nu \left(\frac{-1}{\omega}\right)^\nu \quad \text{as} \quad \omega \to \infty \qquad [B4]$$

The expansion coefficients μ_ν are called generalized moments. The moments μ_ν, $\nu = 0, 1, \ldots$ are related to the short time behavior of $M(t)$ as described by the time derivatives at time $t = 0$

$$(-1)^\nu \mu_\nu = \left.\frac{\partial^\nu}{\partial t^\nu}\right|_0 M(t) \qquad [B5]$$

$$= \frac{1}{(\nu+1)!}\left.\frac{\partial^{\nu+1}}{\partial \sigma^{\nu-1}}\right|_0 \hat{M}(\omega) \qquad [B6]$$

$$= \eta(\mathbf{D} - \mathbf{K})^\nu \mathbf{m}(0) \qquad [B7]$$

where $\sigma = 1/\omega$. The moments μ_ν for $\nu < 0$ are related to the long time behavior through the following expressions

$$\nu!\mu_{-\nu-1} = \int_0^\infty dt\, t^\nu M(t) \qquad [B8]$$

$$= (-1)^\nu \left.\frac{\partial^\nu}{\partial \omega^\nu}\right|_0 \hat{M}(\omega) \qquad [B9]$$

$$= (-1)^{\nu+1}\nu!\eta(\mathbf{D} - \mathbf{K})^{-\nu-1}\mathbf{m}(0) \qquad [B10]$$

By combining Eqs. [B7] and [B10], one can express the moments in powers of the matrix $\mathbf{D} - \mathbf{K}$,

$$\mu_i = (-1)^i \eta(\mathbf{D} - \mathbf{K})^i \mathbf{m}(0) \qquad [B11]$$

where i may be positive or negative.

Evaluation of Observables

The GME approximates $\hat{M}(\omega)$ by a Padé approximant which is designed to reproduce L_l terms in the low frequency expansion and L_h terms in the high frequency expansion. In the time domain, the Padé approximant

corresponds to a sum of exponentials

$$M(t) \approx \sum_{n=1}^{L} a_n e^{-\lambda_n t} \qquad [B12]$$

where $L_h + L_l = 2L$. The connection between the 2L unknowns a_n and λ_n and the moments is given by the 2L relations

$$\sum_{n=1}^{L} a_n \lambda_n^{\nu} = \mu_\nu \qquad [B13]$$

where $\nu = -L_l, -L_l + 1, \ldots, L_h - 2, L_h - 1$. One has then to solve the system of Eq. [B13] to obtain the a_n and λ_n that define the multiexponential approximation of $M(t)$. For example, a monoexponential ($L = 1$) description of $M(t)$ could be given by $L_l = 1, L_h = 1$ which corresponds to the mean-relaxation time approximation.[2] According to Eq. [B13] the parameters a_1 and λ_1 are

$$a_1 = \mu_0, \qquad \lambda_1 = \frac{\mu_0}{\mu_{-1}} \qquad [B14]$$

For a biexponential ($L = 2$) approximation of $M(t)$, Eq. [B13] has been solved (25), and the parameters a_1, a_2, λ_1, λ_2 can be determined as follows (here $m = -L_l$)

$$x = \mu_{m+1}^2 - \mu_{m+2}\mu_m \qquad [B15]$$

$$y = \mu_{m+2}\mu_{m+1} - \mu_{m+3}\mu_m \qquad [B16]$$

$$x = \mu_{m+2}^2 - \mu_{m+3}\mu_{m+1} \qquad [B17]$$

$$\lambda_{1,2} = [y \pm (y^2 - 4xz)^{1/2}]/(2x) \qquad [B18]$$

$$a_{1,2} = (\lambda_{2,1}\mu_{m+2} - \mu_{m+3})/[\lambda_1^{m+2}(\lambda_2 \mp \lambda_1)] \qquad [B19]$$

where first subscripts and upper signs coincide. The quantities x, y, and z measure the deviation from monoexponential behavior; if the decay of $M(t)$ is purely monoexponential, then the moments μ_i will be proportional, i.e., $\mu_i = (\text{const.})\mu_{i+1}$ and x, y, and z will all vanish. For $L > 2$ there is a more practical way to solve Eq. [B13] as presented in ref. 26.

ACKNOWLEDGEMENTS

The authors thank Zan Schulten for originally suggesting this topic, and Joe Schoeniger, Andrew Webb, Zhou Xiaohong, and Jeff Neil for their comments.

REFERENCES

1. N. Haran, M. Shporer, Study of water permeability through phospholipid vesicle membranes by ^{17}O-NMR. *Biochim. Biophys. Acta* **462**, 638–646 (1976).
2. G. Bačić, M. R. Niesman, H. F. Bennett, R. L. Magin, H. M. Swartz, Modulation of water proton relaxation rates by liposomes containing paramagnetic materials. *Magn. Reson. Med.* **6**, 445–458 (1988).
3. S. H. Koenig, Q. F. Ahkong, R. D. Brown, III, M. Lafleur, M. Spiller, E. Unger, C. Tilcock, Permeability of liposomal membranes to water—results from the magnetic field dependence of T_1 of solvent protons in suspensions of vesicles with entrapped paramagnetic ions. *Magn. Reson. Med.* **23**, 275–286 (1992).
4. D. Barsky, B. Pütz, K. Schulten, R. L. Magin, Theory of paramagnetic contrast agents in liposome systems. *Magn. Reson. Med.* **24**, 1–13 (1992).
5. B. Pütz, D. Barsky, K. Schulten, Mechanisms of liposomal contrast agents in magnetic resonance imaging (in forum: liposomes in diagnostic imaging). *J. Liposome Res.* **4**, 771–809 (1994).
6. Keith R. Thulborn, John C. Waterton, Paul M. Matthews, George K. Radda, Oxygenation dependence of the transverse relaxation time of water protons in whole blood at high field. *Biochim. Biophys. Acta* **714**, 265–270 (1982).
7. P. Gillis, S. H. Koenig, Transverse relaxation of solvent protons induced by magnetized spheres: application to ferritin, erythrocytes, and magnetite. *Magn. Reson. Med.* **5**, 323–345 (1987).
8. P. A. Hardy, R. M. Henkelman, Transverse relaxation rate enhancement caused by magnetic particulates. *Magn. Reson. Imaging* **7**, 265–275 (1989).
9. C. Richard Fisel, Jerome L. Ackerman, Richard B. Buxton, Leoncio Garrido, John W. Belliveau, Bruce R. Rosen, Thomas J. Brady, MR contrast due to microscopically heterogeneous magnetic susceptibility: numerical simulations and applications to cerebral physiology. *Magn. Reson. Med.* **17**, 336–347 (1991).
10. K. R. Brownstein, C. E. Tarr, Importance of classical diffusion in NMR studies of water in biological cells. *Phys. Rev. A* **19**, 2446–2453 (1979).
11. G. E. Santyr, I. Kay, R. M. Henkelman, M. J. Bronskill, Diffusive exchange analysis of two-component T_2 relaxation of red blood cell suspensions containing gadolinium. *J. Magn. Reson.* **90**, 500–513 (1990).
12. C. F. Hazelwood, D. C. Chang, B. L. Nichold, D. E. Woessner, Nuclear magnetic resonance transverse relaxation times of water protons in skeletal muscle. *Biophys. J.* **14**, 583–606 (1974).
13. M. E. Fabry, M. Eisenstadt, Water exchange between red cells and plasma: Measurement by nuclear magnetic relaxation. *Biophys. J.* **15**, 1101–1110 (1975).
14. M. E. Fabry, M. Eisenstadt, Water exchange across red cell membranes II. Measurement by nuclear magnetic resonance T_1, T_2, and T_{12} hybrid relaxation: the effects of osmolarity, cell volume, and medium. *J. Membr. Biol.* **42**, 375–398 (1978).
15. J. L. Pirkle, D. L. Ashley, J. H. Goldstein, Pulse nuclear magnetic resonance measurements of water exchange across the erythrocyte membrane employing a low Mn concentration. *Biophys. J.* **25**, 389–406 (1979).
16. R. A. Brooks, J. H. Battocletti, Jr. A. Sances, S. J. Larson, R. L. Bowman, V. Kudravcev, Nuclear magnetic relaxation in blood. *IEEE Trans. Biomed. Eng.* **22**, 12–18 (1975).
17. M. D. Herbst, J. H. Goldstein, Cell water transport measurement by NMR: a three-compartment model which includes cell aggregation. *J. Magn. Reson.* **60**, 299–306 (1984).
18. M. D. Herbst, J. H. Goldstein, A review of water diffusion measurement by NMR in human red blood cells. *Am. J. Physiol.* **256**, C1097–C1104 (1989).
19. W. R. Bauer, K. Schulten, Theory of contrast agents in magnetic resonance imaging: coupling of spin relaxation and transport. *Magn. Reson. Med.* **26**, 16–39 (1992).
20. H. C. Torrey, Bloch equations with diffusion terms. *Phys. Rev.* **104**, 563 (1956).
21. W. Nadler, K. Schulten, Generalized moment expansion for Brownian relaxation processes. *J. Chem. Phys.* **82**, 151–161 (1985).
22. J. Crank, *in* "The Mathematics of Diffusion," 2nd ed., Oxford Science Press, 1975.
23. George E. Forsythe, Wolfgang R. Wasow, *in* "Finite-Difference Methods for Partial Differential Equations," Applied Mathematics Series. John Wiley & Sons, Inc., New York, London, 1960.
24. W. Nadler, P. Tavan, K. Schulten, A model for the lateral diffusion of "stiff" chains in a lipid bilayer. *Eur. Biophys. J.* **12**, 25–31 (1985).
25. Hans-Ulrich Bauer, Klaus Schulten, Walter Nadler, Generalized mo-

[2] Traditionally, the combination of $L_l = 0$, $L_h = 2$ has been employed for monoexponential approximations, mostly because derivatives (cf. Eq. [26]) are often easier to perform than integrals (cf. Eq. [29]), but the use of long-time (negative) moments often yields a much better approximation than the use of only positive moments.

ment expansion of dynamic correlation functions in finite Ising systems. *Phys. Rev. B* **38,** 445 (1988).
26. A. Brünger, R. Peters, K. Schulten, Continuous fluorescence microphotolysis to observe lateral diffusion in membranes: theoretical methods and applications. *J. Chem. Phys.* **82,** 2147–2160 (1985).
27. R. Peters, A. Brünger, K. Schulten, Continuous fluorescence microphotolysis: a new method for the study of diffusion processes in single cells. *Proc. Natl. Acad. Sci. USA* **78,** 962–966 (1981).
28. C. Tilcock, E. Unger, P. Cullis, P. MacDougall, Liposomal Gd-DTPA: preparation and characterization of relaxivity. *Radiology* **171,** 77–80 (1989).
29. E. C. Unger, T. Winokur, P. MacDougall, J. Rosenblum, M. Clair, R. Gatenby, C. Tilcock, Hepatic metastases: liposomal Gd-DTPA-enhanced MR imaging. *Radiology* **171,** 81–85 (1989).
30. R. L. Magin, M. R. Niesman, G. Bačić, The influence of fluidity on membrane permeability: correspondence between studies of membrane models and simple biological systems, *in* "Advances in Membrane Fluidity, Band 4 (R. C. Aloia, C. C. Curtain, L. M. Gorden, Eds.), A. R. Liss, New York, 1990.
31. William F. Windle, "Textbook of Histology," McGraw Hill, New York, 1976.
32. P. Herscovitch, M. E. Raichle, M. R. Kilbourn, M. J. Welch, Positron emission tomographic measurement of cerebral blood flow and permeability-surface area product of water using [^{15}O]water and [^{15}C]butanol. *J. Cereb. Blood Flow Metab.* **7,** 527–542 (1987).
33. O. B. Paulson, M. M. Hertz, T. G. Bolwig, N. A. Lassen, Filtration and diffusion of water across the blood-brain barrier in man. *Microvasc. Res.* **13,** 113–123 (1977).
34. J. O. Eichling, M. E. Raichle, R. L. Grubb, Jr., M. M. Ter-Pogossian, Evidence of the limitations of water as a freely diffusible tracer in brain of the rhesus monkey. *Circ. Res.* **35,** 358–364 (1974).
35. David D. Stark, William G. Bradley, Jr., "Magn. Reson. Imaging," C. V. Mosby, St. Louis, 1988.
36. T. Conlon, R. Outhred, Water diffusion permeability of erythrocytes using an NMR technique. *Biochim. Biophys. Acta* **288,** 354–361 (1972).
37. R. V. Mulkern, A. R. Bleier, T. Sandor, F. A. Jolesz, Compatibility of the two-site exchange model and ^{1}H NMR relaxation rates. *Magn. Reson. Med.* **14,** 377–388 (1990).